Received: 1 May 2022 | Accepted: 16 June 2022

DOI: 10.1002/app.52867

RESEARCH ARTICLE

Applied Polymer SCIENCE WILEY

Superior flame retardancy, antidripping, and thermomechanical properties of polyamide nanocomposites with graphene-based hybrid flame retardant

Kuruma Malkappa[1] | **Jayita Bandyopadhyay**[1] | **Vincent Ojijo**[1] | **Suprakas Sinha Ray**[1,2]

[1]Centre for Nanostructures and Advanced Materials, DSI-CSIR Nanotechnology Innovation Centre, Council for Scientific and Industrial Research, Pretoria, South Africa

[2]Department of Chemical Sciences, University of Johannesburg, Johannesburg, South Africa

Correspondence
Suprakas Sinha Ray, Centre for Nanostructures and Advanced Materials, DSI-CSIR Nanotechnology Innovation Centre, Council for Scientific and Industrial Research, Pretoria 0001, South Africa.
Email: rsuprakas@csir.co.za; ssinharay@uj.ac.za

Funding information
University of Johannesburg, South Africa, Grant/Award Number: 086310; Council for Scientific and Industrial Research, Pretoria, Grant/Award Number: 086ADMIN; Department of Science and Innovation, Grant/Award Number: C6ACH35

Abstract

Graphene is considered one of the most prominent halogen-free multifunctional flame retardants for polymers, and the resultant nanocomposites also display a good balance of properties. However, the biggest concern nowadays is thermal oxidative degradation, which mainly affects the flame retardant (FR) efficiency of graphene. To improve the flame retardancy and thermal oxidative degradation efficiency, graphene was functionalized with a combination of polycyclotriphosphazes and siloxanes via a sol–gel surface modification method, yielding a graphene-based hybrid FR (PSGO) containing multiple elements (P, N, S, and Si). The PSGO-containing PA6 composite exhibited significant improvements in the water resistance, thermal, mechanical, and FR properties, as compared with those of 3-isocyanatopropyltriethoxysilane functionalized graphene oxide (ITS-GO) and siloxane-modified polycyclotriphosphazenes (m-PZS) individually. The peak heat release rate and total heat release values of the PA6 composites with 10 wt% PSGO decreased by 45.7% and 36.9%, respectively, compared to those of pristine PA6. Moreover, it was confirmed that 10 wt% PSGO in the PA6 composite resulting in a V–0 rating in the UL-94 tests, even after the water immersion test. These attractive properties are attributed to the resistance to thermal-oxidative degradation of PSGO and the improved interfacial interactions with the polymer matrix. Therefore, this PSGO can be used as a multifunctional modifier to improve the water resistance, thermal, mechanical, and FR properties of polymers.

KEYWORDS

flame retardance, graphene and fullerenes, mechanical properties, nanotubes, non-polymeric materials and composites, polyamides

1 | INTRODUCTION

Polyamide 6 (PA6) is an engineered polymer that is widely used in several advanced technical applications, including electrical, electronics, automotive production, and telecommunication, owing to its excellent mechanical properties, high heat transition temperature, and attrition resistance.[1,2] Unfortunately, PA6 is extremely flammable with severe melt dripping and rapid flame propagation, and it releases considerable amount of

dense toxic smoke during combustion,[3] posing a significant threat to human lives, safety, and property. Environmentally friendly, halogen-free inorganic nanomaterials with a layered structure and high aspect ratio, such as nanoclay,[4,5] graphene,[6,7] layered double hydroxides,[8] and metal sulfides,[9,10] are considered to be more effective flame retardant (FR) additives. Graphene with a high aspect ratio, high surface area, and good thermal and mechanical properties has great potential as an FR additive for polymers.[11,12] However, the poor compatibility of graphene oxide (GO) with polymer matrices, nonuniform dispersion, and weak charring ability limit its FR efficiency. Hence, it is important to functionalize GO with appropriate flame-retardant compounds, such as P, P–N, and P–N–Si containing compounds.

Polycyclotriphosphazene (PZS) compounds are well-known cross-linking FR additives for polymers to improve their FR activity.[13,14] Their structure contains alternately connected P and N with conjugated double bonds in the hexatomic ring, which enhances the FR activity with possible synergistic action in the condensed and gas phases. Different types of cyclotriphosphazene-grafted GO nanosheets were successfully synthesized and confirmed to be more effective FRs for various polymers.[10,15] Feng et al.[16] successfully synthesized P and N co-doped rGO (PN-rGO), which effectively improved the FR activity of epoxy resin (EP). GNS@PDA@HPTCP was shown to be a more effective FR for thermoplastic polyurethane (TPU), which was obtained from graphene sheets alternately reacting with polydopamine, hexachloro cyclotriphosphazene (HCCP), and hydroquinone. The TPU composite with 2 wt% exhibited a 59.6% reduction in the peak heat release rate (pHRR) value compared with that of pristine TPU.[17] Similarly, Hu et al.[18] reported that hyperbranched FR-functionalized GO nanosheets (FGOs) improved the fire safety of polystyrene (PS). They confirmed that the FR functionalization of GO nanosheets significantly improved their dispersion and barrier properties. However, the strength and thermal oxidative degradation resistance of GO with P-, N-, and P-N-containing compounds are insufficient to resist further material burning at higher temperatures in real fire scenarios.

In this direction, researchers have modified the FRs using organo siloxane compounds and established that silica plays a significant role in the condensed phases as char insulator and reinforcer by forming Si–O–Si bonds at the high temperature regions during combustion.[6,19–21] Wang et al.[22] successfully synthesized nanosilica-functionalized GO nanosheets (m-SGO) from tetraethyl orthosilicate (TEOS) and aminopropyl triethoxysilane (APTES). They confirmed that the EP composite with 1.5 wt% of m-SGO yielded significantly improved thermal stability and mechanical and flame-retardant properties. Tang et al.[23] successfully synthesized a GO-functionalized phosphorous-polyhedral oligomeric silsesquioxane (P-POSS-GO) hybrid FR and used it to prepare bismaleimide resin composites. They observed that 4 wt% of P-POSS-GO containing a bismaleimide composite exhibited better FR activity with a V–0 rating. Fan et al.[24] synthesized a novel aromatic Schiff base-containing branched polysiloxane (PCNSi) and used it to prepare PA6 composites with various weight percentages (2, 4, and 6). The flammability results revealed that the PA6/PCNSi-6% composite exhibited a 48.9% reduction in the pHRR compared to that of pristine PA6 and yielded a desirable V–0 rating in the UL-94 test. Moreover, good compatibility between the polymers and siloxane compounds can improve the flame retardancy and physical properties of the composites. Based on aforementioned literature, functionalized GO containing P, N, and Si is expected to be a more promising FR additive for PA6 polymers. However, the problem of water absorbability of FRs must be addressed because it seriously deteriorates the flame retardancy and processability. To develop strong graphene-based FRs with high FR efficiency, excellent water resistance is imperative for polymer materials. Polydimethylsiloxane (PDMS), which has exceptional characteristics that improve flame retardancy and hydrophobicity, is commonly used to modify various nanofiller surfaces for fabric coatings.[25,26] For instance, the use of PDMS for surface functionalization of aluminum diethylphosphinate (ADP) yielded the (PDMS-ADP) FR for fabricating PA6 FR composites.[27] The results revealed that the presence of PDMS improved the ADP hydrophobicity and FR activity of PA6 composites. It was also confirmed that the PA6 composite modified with 12 wt% PDMS-ADP exhibited a V–0 rating in the UL-94 test. Xu et al.[28] prepared modified aluminum hypophosphate (MAHP) utilizing the P–H bond of aluminum hypophosphate and an aldehyde group of cyclotriphosphazenes, and added it to PA6 as a FR. The PA6 composite with 21 wt% MAHP retained its superior FR activity even after the water immersion test with a V–0 rating in the UL-94 test. Graphene-based materials with combined properties, such as flame retardancy and hydrophobicity, have aroused new interest for coatings and polymer composites.[29,30]

To overcome all the above issues and to achieve flame retardancy and hydrophobicity by improving the thermal oxidative degradation of graphene sheets, a polycyclotriphosphazene-siloxane functionalized graphene (PSGO) hybrid FR was successfully synthesized via the sol–gel method. Here, APTES and PDMS were used to modify the PZS microspheres, and the product was subsequently used to functionalize the surface of 3-isocyanatopropyltriethoxysilane functionalized GO

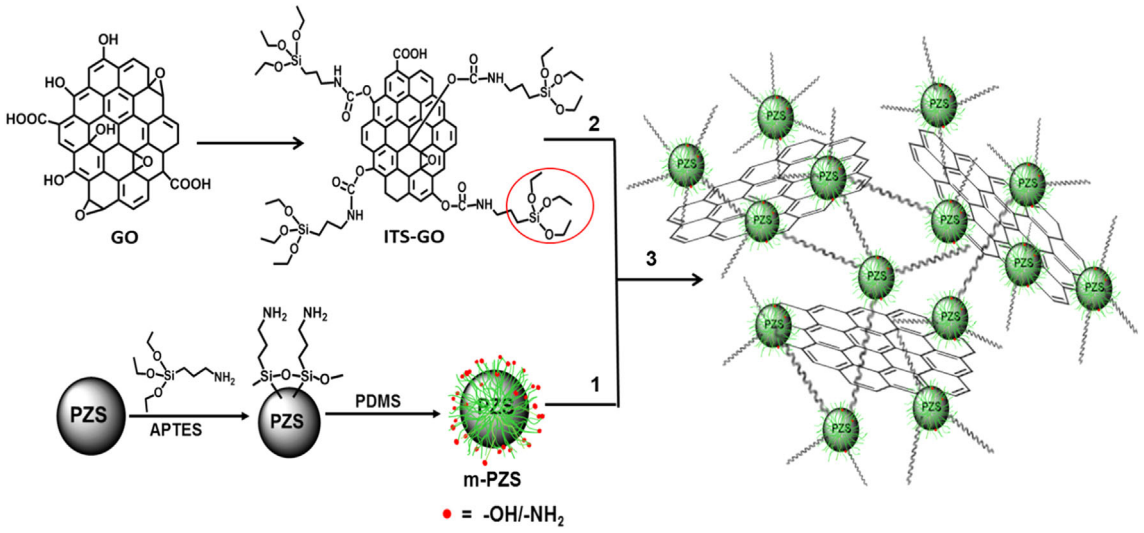

SCHEME 1 Synthesis method for the PSGO hybrid flame retardant. [Color figure can be viewed at wileyonlinelibrary.com]

(ITS-GO) nanosheets for obtaining a hybrid organic/inorganic FR PSGO. Graphene containing P, N, S, and Si can decrease the flammability of polymers. To the best of our knowledge, no reports have been published on the simultaneous modification of graphene with multiple P, N, S, and Si elements for flame retardancy and hydrophobicity of PA6 composites. Hence, we synthesized a supramolecular graphene-based hybrid FR PSGO with significantly enhanced FR activity and hydrophobicity of the PA6 polymer. Accordingly, a series of PSGO-containing PA6 composites was processed with varying PSGO loadings of 3, 5, and 10 wt%. To compare the FR efficiency of PSGO with others FRS, PA6 composites containing 10 wt% m-PZS and ITS-GO were also processed. The flammability, toxic gas evolution, and water-resistant behavior of various composites were thoroughly investigated using cone calorimetry, UL-94, TG-FTIR, and water-impregnated method.

2 | EXPERIMENTAL

2.1 | Materials

PA6 1030 B was supplied by Ube Industries Ltd., Tokyo, Japan. 4, 4′-dihydroxydiphenyl sulfone (BPS), HCCP, and trimethylamine (TEA) were purchased from Sigma Aldrich, South Africa. Acetonitrile, tetraethyl orthosilicate (TEOS), hydroxyl-terminated PDMS, ITS, APTES, and dimethyl formamide (DMF) were purchased from Minema Chemicals, South Africa. The chemicals were used as received without further purification.

2.2 | Preparation of m-PZS

PZSs were prepared according to our previously reported method.[2,31] and they contain terminal hydroxyl groups that are useful for further surface modification with suitable compounds. The surface modification procedure was as follows: 2 g of PZS microspheres were dispersed into a 300 ml mixture of APTES/water/ethanol (vol/vol/vol = 1/1/18), and the resulting solution was refluxed at 70°C for 3 h. Subsequently, 2 g of PDMS and 2 ml of 20% HCl were added alternately, and stirring was continued for 24 h. Finally, the obtained white suspension product was centrifuged and washed with water and ethanol. As presented in Scheme 1, functionalization of PZS by converting the surface hydroxyl groups into amino groups was carried out using APTES, and further condensation reactions between APTES and PDMS occurred on the surface of the PZS microspheres in the presence of an acidic medium.[32]

2.3 | Synthesis of ITS-GO and PSGO

GO nanosheets were synthesized following the improved Hummers method.[33] Briefly, 1 g of GO was dispersed in 300 ml of DMF and sonicated for 1 h to increase the GO dispersion level. Then, 2 ml of ITS was dropped into the GO solution under nitrogen atmosphere and stirred for 1 h. Subsequently, 20 µl of dibutyltin dilaurate (DBTDL) was added to the reaction mixture and the stirring was continued for another 2 h at 80°C. After the reaction, 1 g of m-PZS dispersed in 100 ml of ethanol was added slowly to the reaction mixture over 1 h. Then,

ammonium hydroxide solution was added to the reaction mixture and stirred for 24 h at 70°C. The resulting product was centrifuged and washed with ethanol and water. The final product was dried in an oven at 90°C for 24 h and designated as PSGO. Scheme 1 shows the complete synthesis route of graphene-based hybrid FR PSGO.

2.4 | Preparation of PA6 composites with different FR compounds

The PA6, ITS-GO, m-PZS, and PSGO compounds were dried in an oven at 80°C overnight before extrusion. Then, PA6 composites were prepared with different FR compounds using a melt-blending process. To process the composites, a co-rotating twin-screw extruder (Process 11, $L/D = 40$, Thermo Scientific) was used, and all extruded samples were collected using a water bath and pelletized. The temperature profiles for the different zones were set at 120, 240, 250, 260, 260, 260, and 260°C, whereas the die temperature was set to 250°C. The screw speed was set at 200 rpm. The pellets were subsequently compression-molded at 240°C using a 9 MPa presser (Carver, model-3851-0) for 6 min. The obtained samples were characterized further.

2.5 | Characterization and property measurements

The Fourier transform infrared (FTIR) spectra of the samples were obtained using a PerkinElmer FTIR spectrometer (Spectrum 100) in the transmission mode over a wavelength range of 600–4000 cm^{-1}, and 32 scans were collected at a resolution of 4 cm^{-1}. The X-ray diffraction (XRD) patterns of the synthesized powder samples, such as PZS, m-PZS, and PSGO, were collected from the X-ray generator using a PANalytical X'pert PRO diffractometer (Netherlands) and Cu Kα radiation ($\lambda = 0.154$ nm, current = 30 mA, and voltage = 40 kV). The diffractograms were collected at a scan rate of 0.6 min^{-1} within a 2θ range of 2–80°. The thermal stability and released degradable volatile components from PA6 and its composites with m-PZS, ITS-GO, and PSGO at different weight percentages were evaluated using a TGA-FTIR/py-GC/MS with a PerkinElmer Pyris 1 TGA thermogravimetric analyzer connected to a Nicolet IS50 spectrometer within the temperature range of 50–800°C at a heating rate of 20°C min^{-1} under air and nitrogen environments. Each sample weighed approximately 20 mg. The flammability properties of PA6 and its composites with m-PZS, ITS-GO, and PSGO at different weight percentages were studied using cone colorimetry (Fire Testing Technology, East Grinstead, UK), according to ISO 5660. All compression-molded samples ($100 \times 100 \times 3$ mm^3) were wrapped in aluminum foil with the top part of the sample open and exposed to a radiant cone at a heat flux of 25 kW m^{-2}. The vertical burning test, UL-94, was carried out using a model UL-94 (Fire Testing Technology Limited, UK). The samples with dimensions $125 \times 13 \times 3.2$ mm^3 were prepared using the compression-molded method, and the flame chamber was maintained according to ASTM D5207-03. To determine the water resistance of PA6 and its composites with various FR contents, the samples were immersed in distilled water at 70°C for 168 h to obtain water-treated samples. The water was changed every 24 h according to UL746C. For each sample, the initial weight was considered as W_0. After 168 h, the water-treated samples were dried in a vacuum oven at 90°C for 48 h, and weight of the sample was considered as W_1. The mass loss percentage (MLP) of the specimen was measured using the following equation:

$$\mathrm{MLP} = \left[\frac{(W_0 - W_1)}{W0}\right] \times 100 \quad (1)$$

The thermomechanical properties of the compression-molded samples of PA6 and its composites were evaluated using a dynamic mechanical analyzer (DMA, PerkinElmer 8000) in single bending mode over a temperature range of −100 to 100°C with a temperature scan of 2°C min^{-1} at a frequency of 1 Hz and a strain amplitude of 0.05%. The microstructures of the char residues obtained from the cone colorimetry test were analyzed using scanning electron microscopy (SEM; AURIGA Crossbeam workstation, Carl Zeiss, Germany) at 3 kV. Raman spectra of char residues were obtained using the 514.5 nm line of a Lexel Model 95-SHG argon ion laser as the excitation source and a Horiba Lab RAM HR Raman spectrometer equipped with an Olympus BX41 microscope attachment. Raman spectra for each sample were obtained for integration times of 60 s. The X-ray photoelectron spectroscopy (XPS) spectra were obtained using a Thermo Scientific spectrometer (model: ESCALAB 250XI) with an XR6 micro-focused monochromator (Al Kα) X-ray source.

3 | RESULT AND DISCUSSION

3.1 | Characterization of synthesized FRs

In this work, a novel PZS-based derivative (m-PZS) containing P, N, S, and Si was synthesized by functionalizing ITS-GO to obtain a more efficient siloxane-cross-linked hybrid GO-based FR (PSGO), as shown in

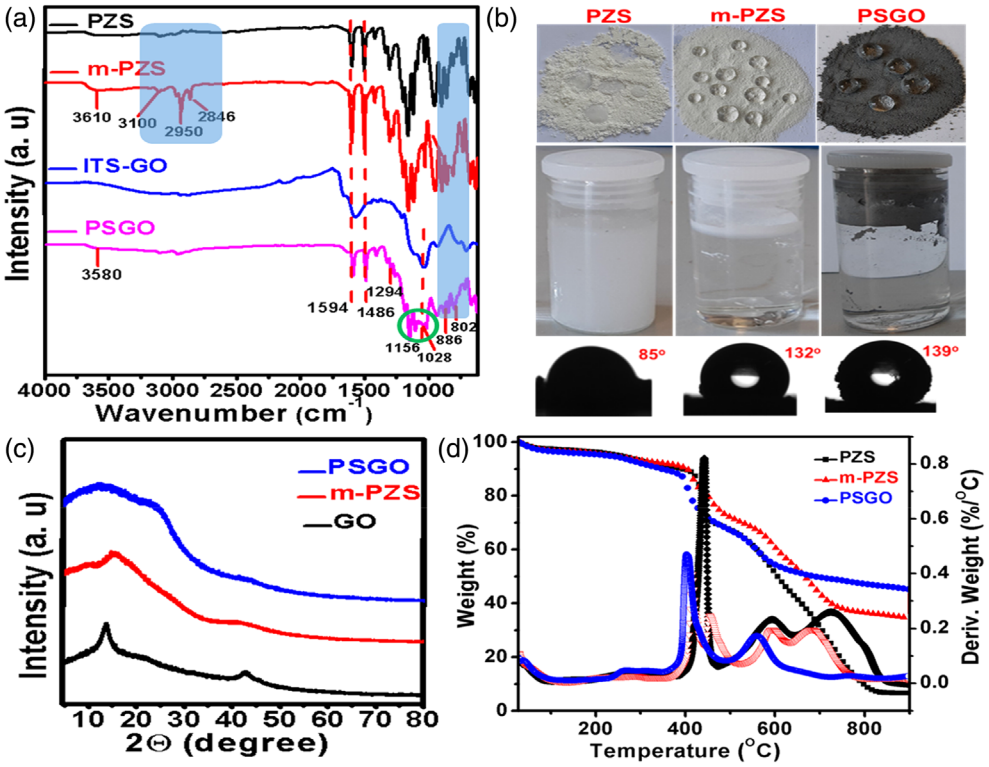

FIGURE 1 FTIR spectra (a) photographs of water droplets on the surface of powder samples immersed in water and respective contact angles images; (b) XRD plots (c) and TGA plots (d) of ITS-GO, m-PZS, and PSGO. [Color figure can be viewed at wileyonlinelibrary.com]

Scheme 1. Figure 1a shows the FTIR spectra of the PZS, m-PZS, ITS-GO, and PSGO. The typical peaks of PZS in the FTIR spectrum are observed at 1158 and 886 cm^{-1}, which are attributed to the P═N and P–N characteristic peaks of the cyclotriphosphozene ring, respectively.[2,34] Moreover, the sharp peaks at 1486 and 1594 cm^{-1} are attributed to the phenyl group of BPS, and the peaks at 1158 and 1294 cm^{-1} are attributed to the O═S═O groups of BPS.[35] After siloxane functionalization, the FTIR spectra (Figure 1a) clearly exhibited new peaks for m-PZS at 2840 and 2956 cm^{-1} (symmetric and asymmetric stretching vibrations of PDMS alkyl C–H), and at 3100 and 3610 cm^{-1} corresponding to the amine N–H and O–H groups, respectively, along with all the characteristic peaks of PZS.[2] However, the FTIR spectrum of PSGO changed significantly, except for the characteristic peaks of PZS. The new peak observed at 1060–1108 cm^{-1} corresponds to Si–O–Si and Si–O–C asymmetric stretching vibrations, as shown in Figure 1a. Moreover, the peaks at 946 and 804 cm^{-1} correspond to Si–OH stretching vibrations and Si–O–Si bending vibrations, respectively, while the important –NCO peak at 2270 cm^{-1} is not observed in the PSGO spectrum.[36] Hence, these results indicate that m-PZS was successfully grafted onto the surface of ITS-GO by the formation of highly cross-linked urethane-siloxane functionalities.

The wettability of PZS, m-PZS, and PSGO was analyzed by water sedimentation and contact angle tests, and the corresponding images are presented in Figure 1b. The water droplets on the surface of the PZS powder were immediately absorbed, and they also sank to the bottom of the container with a corresponding contact angle of 85°. These observations indicate that PZS is hydrophilic because of its molecular polarity. A combination of PDMS and APTES was used for surface modification to increase the hydrophobicity and flame retardancy of the PZS. The PDMS mainly reduces the surface energy owing to its alkyl chains, resulting in an increase in hydrophobicity. The resulting m-PZS exhibited super-hydrophobicity, as shown in Figure 1b. The water droplets on the surface of m-PZS are spherical, and when dispersed in water, they are suspended stably on top of water for a long time, with a contact angle of 132°. To further increase the FR activity, m-PZS was bonded on the ITS-GO nanosheets in a suitable way by creating reactive siloxane functionalities. The derived hybrid FR PSGO also exhibited super-hydrophobicity with a contact angle of 139°, and was also suspended stably in water, similar to m-PZS, as shown in Figure 1b.

Figure 1c shows the XRD spectra of the GO, m-PZS, and PSGO. In the XRD pattern of the pristine GO, a diffraction peak is observed at $2\theta = 12.3°$ corresponding to the (002) plane. The XRD pattern of amorphous m-PZS shows a broad peak around $2\theta = 15°$. However, after m-PZS functionalization of the GO surface, the diffraction peak of GO is slightly downshifted to $2\theta = 10.5°$ with broadening of the peak. Moreover, the newly generated

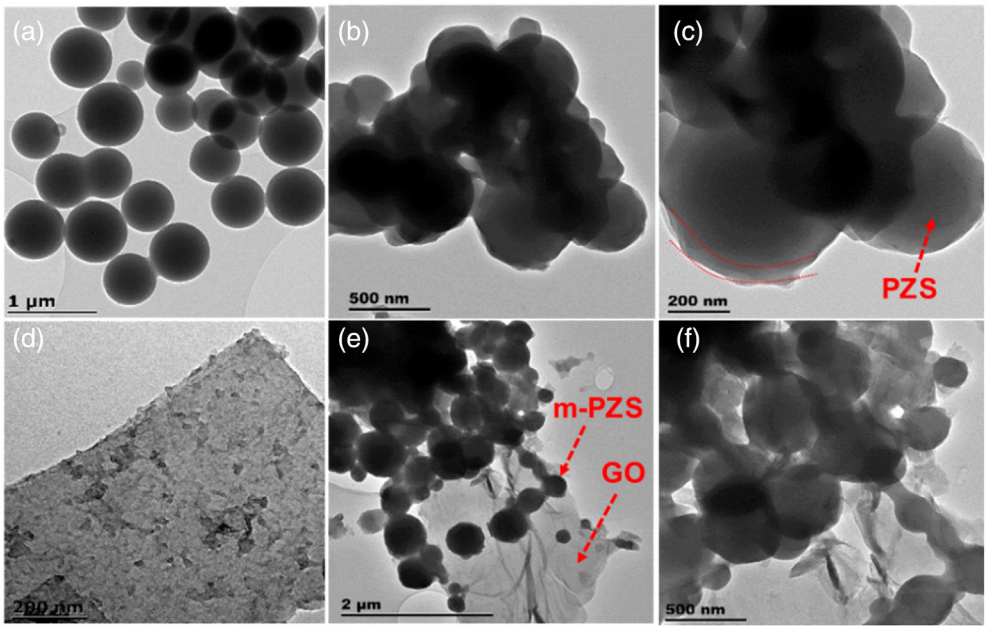

FIGURE 2 TEM images of (a) PZS; (b, c) m-PZS, (d) ITS-GO, and (e, f) PSGO with different magnifications. [Color figure can be viewed at wileyonlinelibrary.com]

amorphous broad peak is located at approximately $2\theta = 20–25°$, indicating the formation of a bridge between the reactive functional groups of m-PZS and GO nanosheets. To determine the thermal stability and effect of m-PZS grafting on GO nanosheets, TGA analysis was carried out for all samples of ITS-GO, m-PZS, and PSGO, and the obtained plots are shown in Figure 1d. All samples exhibited similar trends in thermal degradation behavior, except for maximum decomposition and residual char percentages. As seen from the TGA plots of ITS-GO, the maximum decomposition occurred at 420°C, and the char residue remaining at 900°C was 8%. The maximum decomposition temperature of m-PZS is slightly higher than that of ITS-GO. Furthermore, the char residue of m-PZS at 900°C was 32%, which is significantly higher than that of ITS-GO. This is attributed to the formation of highly cross-linked silicate compounds between APTES and PDMS on the surface of PZS.[26] However, after m-PZS was grafted onto the surface of the ITS-GO nanosheets, the char residue at 900°C was 45%, which is significantly higher than those of ITS-GO and m-PZS. This is attributed to the fact that ITS-GO nanosheets provide a strong physical barrier against the thermal degradation of m-PZS at high temperatures.

The morphologies and microstructures of PZS, m-PZS, ITS-GO, and PSGO are shown in Figure 2. The TEM image of PZS in Figure 2a clearly shows that PZS formed uniform spherical particles. Parts (b) and (c) of Figure 2 present the TEM images of m-PZS, which exhibit a clear difference from PZS. During surface modification, silanol crosslinking occurs on the surface of PZS microspheres between the terminal siloxane functionalities of APTES/PDMS and the hydroxyl groups of PZS. These cross-linked siloxanes uniformly functionalized on the surface of PZS are indicated by red marks in the figure. The TEM images of the graphene-based hybrid FR PSGO (Figure 2e,f) clearly show that the m-PZS microspheres are tethered on the surface of the graphene sheets with the formation of cross-linked siloxane functionalities. This is because the PZS microspheres were modified with APTES/PDMS, resulting in PZS containing terminal —OH/—NH_2 groups on its surface that can react with the —COOH/OEt terminal groups of ITS-GO to finally form a multi-functionalized graphene-based hybrid FR, as shown in Scheme 1.

3.2 | Thermal stability

The thermal stability of pristine PA6 and its FR composite samples was analyzed by TGA in nitrogen and air atmospheres. The resulting TGA curves are presented in Figure 3 and the corresponding data are listed in Table 1. As shown in Figure 3, pristine PA6 and its composites with different FRs exhibit the same thermal degradation phenomenon. Single-stage thermal degradation of the samples at 380–450°C was observed in the presence of nitrogen, corresponding to the degradation of PA6 chains. However, in air atmosphere, there was additional mass loss at 480–620°C owing to the oxidative degradation of unstable char. The temperatures at 10 wt% weight loss ($T_{-10\%}$), 70 wt% weight loss ($T_{-70\%}$), and the percentage of residual char at 750°C are listed in Table 1 to compare the thermal degradation behavior of the PA6 FR composites. Figure 3a shows that the $T_{-10\%}$ and $T_{-70\%}$ of pristine PA6 are 408.5 and 456.2°C, respectively.

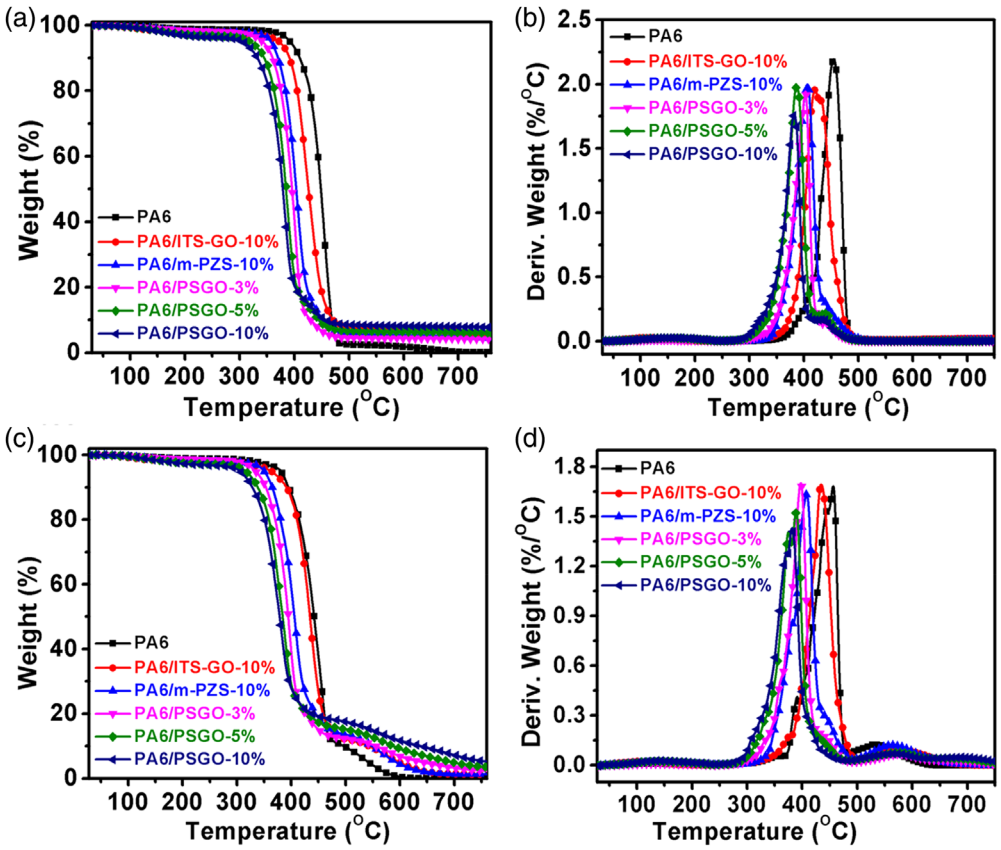

FIGURE 3 TGA and DTG plots of PA6 and its composites with different FR content; (a, b) under nitrogen and (c, d) under air environment. [Color figure can be viewed at wileyonlinelibrary.com]

TABLE 1 TGA and DTG data of pristine PA6 and its composite in under nitrogen and air atmospheres.

	N_2 atmosphere				O_2 atmosphere			
Samples	$T_{-10\%}$ (°C)	$T_{-70\%}$ (°C)	Char at 750 °C (%)	α_{max} (%/ °C)	$T_{-10\%}$ (°C)	$T_{-70\%}$ (°C)	Char at 750°C (%)	α_{max} (%/°C)
PA6	408.5	456.2	0.2	2.1	395.4	455.1	0.1	1.6
PA6/ITS-GO-10%	394.3	438.6	4.3	1.6	391.3	447.3	0.9	1.6
PA6/m-PZS-10%	366.4	413.7	3.8	1.9	365.7	421.5	1.1	1.5
PA6/PSGO-3%	358.3	405.1	4.8	2.3	351.1	406.6	2.4	1.9
PA6/PSGO-5%	347.2	393.6	7.5	1.9	337.0	395.1	4.1	1.5
PA6/PSGO-10%	328.9	387.2	8.9	1.8	321.5	393.2	6.2	1.4

The $T_{-10\%}$ values for all FR PA6 composites under both nitrogen and air conditions were lower than that of pristine PA6. The thermal stabilities of the composites containing hybrid PSGO were lower than those of the composites containing ITS-GO and m-PZS FRs individually. An increase in the percentage of PSGO in the PA6 composite results in a decrease in the $T_{-10\%}$ values. The $T_{-10\%}$ and $T_{-70\%}$ values of PA6/PSGO-10% composite under nitrogen are 328.9 and 387.2°C, respectively. This was mainly due to the synergistic charring effect of ITS-GO and m-PZS. In the differential thermogravimetric analysis (DTG) plots shown in Figure 3b,d, the α_{max} (conversion at the maximum conversion rate $[d\alpha/dt]_{max}$, Table 1) decreased with decreasing peak intensity from pristine PA6 to the PA6/PSGO-10% composite. This indicates that PSGO promotes PA6 degradation at lower temperatures, which results in the formation of thermally insulating char, thus inhibiting further polymer degradation. Consequently, the char residues at 750°C from the pristine PA6 to the PA6/PSGO-10% composite increased from 0.2% to 8.9%. The significant improvement in the char yield is mainly attributed to the positive synergetic association of the m-PZS and ITS-GO nanosheets.

The other reason for constructing a ternary graphene-based hybrid FR PSGO is to improve the interfacial interactions and dispersion level of the FR in the polymer

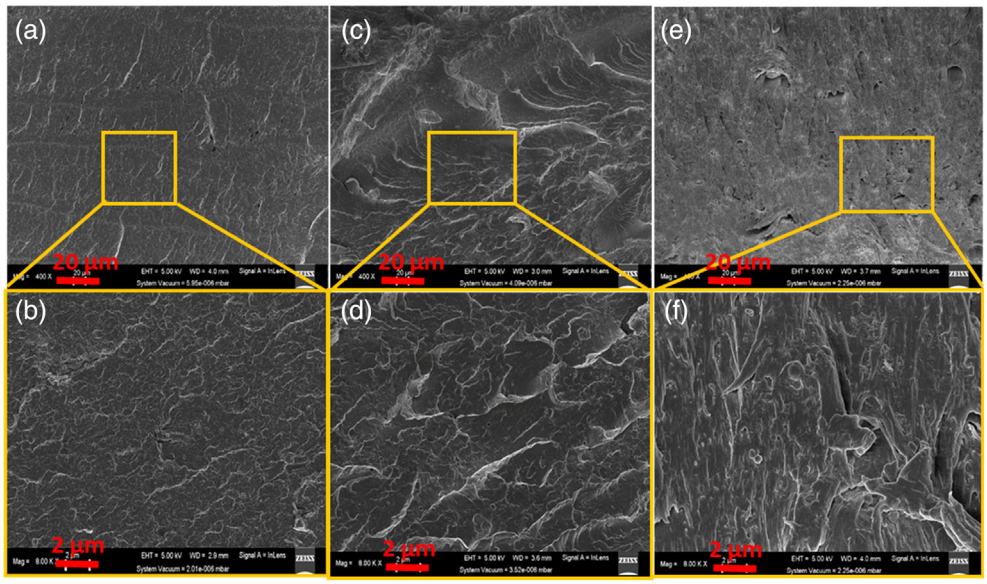

FIGURE 4 SEM micrographs of the fractured surface of pristine PA6 (a,b), PA6/ITS-GO-10% (c,d), and PA6/PSGO-10% (e,f). [Color figure can be viewed at wileyonlinelibrary.com]

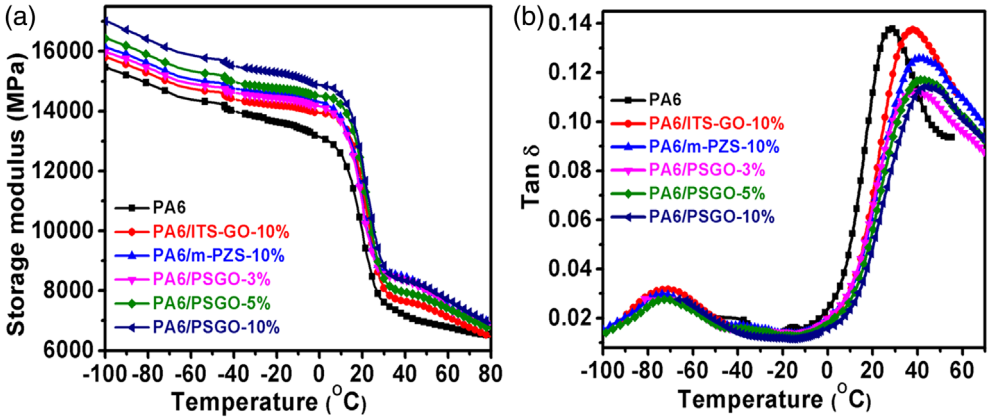

FIGURE 5 (a) Storage modulus and (b) tan δ plots of PA6 and its nanocomposites with different FR compounds. [Color figure can be viewed at wileyonlinelibrary.com]

matrix, which could in turn enhance the fire retardancy and mechanical properties of the polymer material. The surface microstructures of freeze fractured PA6 and its composites with various FR compounds are presented in Figure 4. Noticeable differences were observed between the pristine PA6 and the PA6 composites containing ITS-GO and PSGO. Pristine PA6 shows a smooth surface in Figure 4a,b, whereas a wrinkled structure is observed in Figure 4c,d for the PA6 composite with ITS-GO. This indicates that the ITS/GO nanosheets were tightly embedded in the polymer matrix. Furthermore, a smoother morphology is observed with the collapse of the wrinkling structure for the PA6/PSGO-10% composite, as shown in Figure 4e,f. This is due to the better dispersion of PSGO in the PA6 matrix, as a result of siloxane cross-linked PZS functionalized on the surface of ITS-GO nanosheets, which are capable of increasing the interfacial interactions between the PSGO and PA6 polymer matrix, resulting in enhanced mechanical properties and fire retardancy of the PA6 composite.

Owing to their high aspect ratio and excellent mechanical strength, GO nanofillers and their derivative compounds have been widely reported to improve the thermomechanical properties of polymer composites as compared to those of the host polymer.[37–39] With the addition of GO to the polymer matrix, GO acts as a primary load-bearing component in the polymer composite, improving the mechanical properties.[10,40] The effect of the hybrid FR PSGO nanofillers on the dynamic mechanical properties of the PA6 composites was analyzed using a DMA, and the resulting curves are shown in Figure 5a, b. The addition of ITS-GO, m-PZS, and PSGO into the PA6 matrix resulted in an improvement in the storage modulus (E′). The increase in E′ for PA6 containing PSGO was higher than that for the composites with ITS-GO and m-PZS, both in the glassy and rubbery regions. Moreover, an increase in the percentage of PSGO led to an increase in E′ values. For instance, in the glassy region, the E′ for PA6/PSGO-10% composite was 1710 MPa at −100°C, compared to 1560, 1580, and

1610 MPa for the pristine PA6, PA6/ITS-GO-10% and PA6/m-PZS-10% composites, respectively. This is mainly attributed to the possible internal crosslinking between the polymer matrix and PSGO hybrid nanofiller; the degree of crosslinking increases with increasing PSGO content in the PA6 composite, and thus strengthening the storage energy.[22,41] The tan δ plots (Figure 5b) clearly show two peaks corresponding to the α and β for pristine PA6 and its FR composites, as explained in our previous work.[42] The β transition peak is observed at approximately $-75^{\circ}C$ owing to the damping of carbonyl group of PA6, which is in part of formation of hydrogen bonds with absorbed water. The α transition appeared at a higher temperature with a high peak intensity and was considered as the glass transition temperature (T_g). The T_g for pristine PA6 was observed at 29°C, and for all the PA6 composites, it shifted to higher temperatures, as shown in Figure 5b. The PSGO containing PA6 composites had higher T_g values (approximately 34°C) with decreased peak intensities compared to that of pristine PA6. Moreover, the T_g values increased with increasing PSGO content. This indicates that in the presence of PSGO, the interfacial interactions between PSGO and PA6 were improved, increasing the rigidity of the polymer chains.

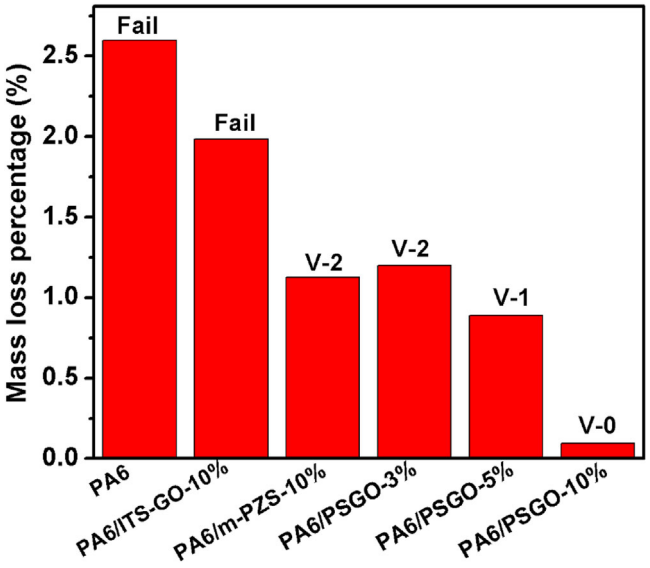

FIGURE 6 Mass loss percentage and UL-94 test results of PA6 and its composites with different FR compounds after water treatment. [Color figure can be viewed at wileyonlinelibrary.com]

3.3 | Water resistance and UL-94 analysis

To evaluate the water resistance behavior of the PA6 composites with various FR contents, the samples were immersed in hot water at 75°C for 168 h, and the resulting MLP data are shown in Figure 6 and Table 2. In fact, the water absorbability of FRs restricts their application in polymer composites owing to a decrease in flame retardancy and processing ability.[43,44] The FR extraction of MLP values mainly depends on the hydrophobic nature of the FR in the PA6 composites; if the FR is more hydrophobic, the extraction of FR is lower, which contributes to the excellent FR activity even after water treatment. As shown in Figure 6, the MLP value for the PA6/ITS-GO-10% composite is 1.9%, which is higher than that for the PA6/m-PZS-10% composite (1.2%). This can be attributed to the more hydrophilic nature of ITS-GO compared to that of m-PZS, which allows a higher amount of water to circulate inside the PA6 composite through the material surface, leading to a greater extraction of FR from the composite. However, the MLP values of the PA6 composite containing the hybrid FR PSGO significantly decreased. An increase in the PSGO content resulted in a further decrease in the MLP values, with the PA6 composite containing 10 wt% PSGO exhibiting the lowest MLP value of 0.1%. This indicates that at this percentage, there was sufficient PSGO in the PA6 composite to prevent water absorption. The

TABLE 2 Water resistance and UL-94 test results

Sample	MLP $= \left[\frac{(W_0 - W_1)}{W_0}\right] \times 100$	Before water treatment		After water treatment	
		Melt dripping	UL-94 rating	Melt dripping	UL-94 rating
PA6	3.4	Y	Fail	Y	NR
PA6/ITS-GO-10%	1.9	Y	V–2	Y	NR
PA6/m-PZS-10%	1.2	Y	V–2	Y	V–2
PA6/PSGO-3%	1.3	N	V–1	Y	V–2
PA6/PSGO-5%	0.8	N	V–1	N	V–1
PA6/PSGO-10%	0.1	N	V–0	N	V–0

Abbreviations: MLP, mass loss percentage; NR, no ratting.

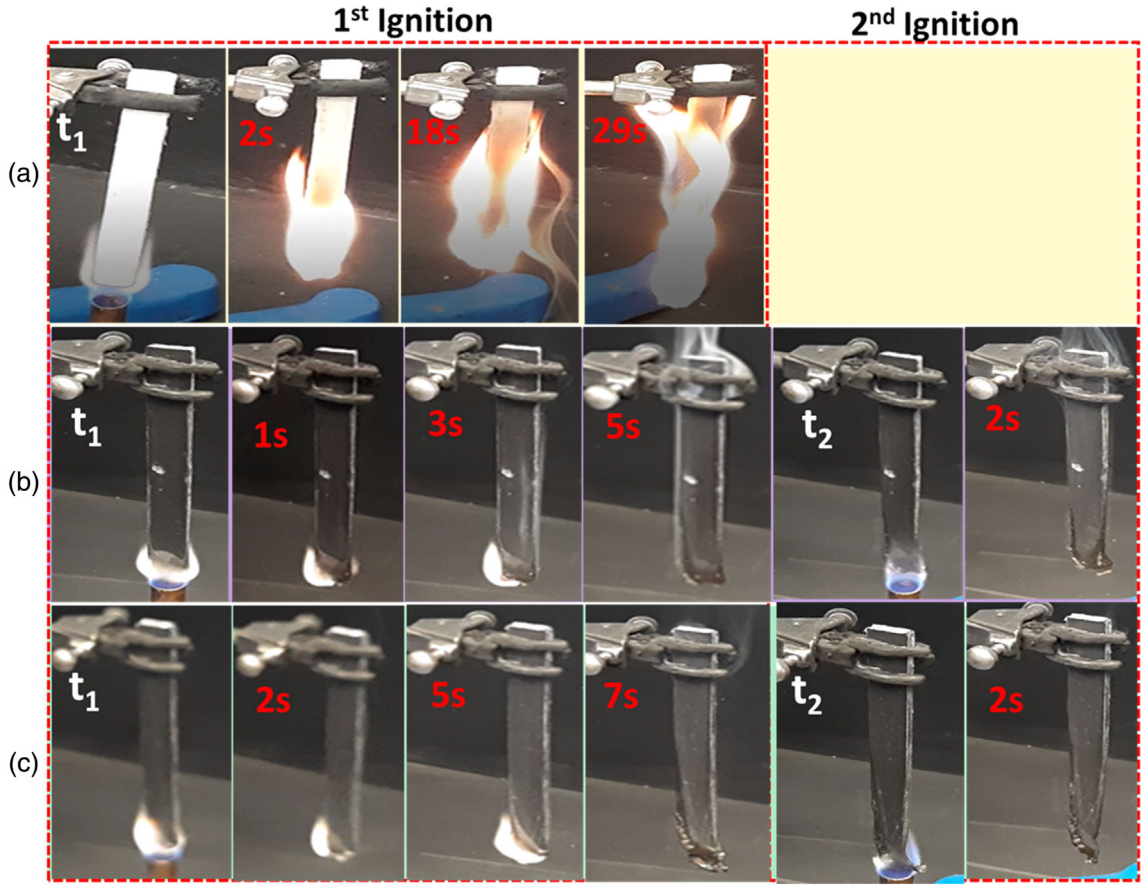

FIGURE 7 UL-94 test burning images of water treated samples: Pristine PA6 (a), PA6/PSGO-10% composite samples before water treatment (b) and after water treatment (c). Credit: Kuruma Malkappa (first author) [Color figure can be viewed at wileyonlinelibrary.com]

UL-94 test burning behavior images for the corresponding water-treated pristine PA6 and PA6/PSGO-10% composites before and after water treatment are shown in Figure 7. The UL-94 test results revealed that there was no significant difference in the flammability behavior even after water treatment of the PA6/PSGO-10% composite, except for slight differences observed in the PA6/PSGO-3% composite. The PSGO content of 3 wt% was not sufficient to prevent water absorption. Hence, the PA6/PSGO-3% composite attained a V–2 rating after water treatment instead of a V–1 rating, as shown in Table 2. However, at 10 wt% loading, sufficient PSGO was present in the PA6 composite, which contributed to the excellent water resistance and superior flame retardancy by attaining the V–0 rating in the UL-94 test, even after water treatment, as shown in Figure 7c.

3.4 | Flammability analysis

A cone colorimetry test was performed to assess the combustion behavior of PA6 and its composites containing ITS-GO, m-PZS, and PSGO under full-scale fire conditions. The fire parameters necessary for the analysis of FR properties, such as heat release rate (HRR), THR, time to ignition (TTI), and time to $_{P}$HRR (t_{PHRR}) are listed in Table 3. The HRR is an important parameter for assessing the fire intensity of a material, and lower HRR values indicate better fire safety.[22] The HRR and THR versus time plots for PA6 and its composites are shown in Figure 8a,b, and all the corresponding data obtained are presented in Table 3. From the HRR plots and Table 3 data, a clear difference is observed for the $_{P}$HRR and TTI values from the pristine PA6 to the PA6 composite. In Figure 8a, the HRR value of pristine PA6 rapidly increased to 514.3 kW m^{-2}, while the corresponding TTI value was 91.6 s. With the addition of 10 wt% ITS-GO and m-PZS into the PA6, the $_{P}$HRR values of PA6 composites were decreased to 477.6 and 438.3 kW m^{-2}, respectively, with a decrease in the TTI values. The presence of ITS-GO and m-PZS accelerated the degradation of the polymer chain, leading to rapid burning. Similarly, after the incorporation of hybrid FR PSGO into the PA6 matrix, a considerable decrease in the $_{P}$HRR values was observed. An increase in PSGO content resulted in a decrease in the pHRR values. The $_{P}$HRR value for the

TABLE 3 Cone calorimetry test data of PA6 and its composites obtained from flammability test.

Sample	$_{p}$HRR (kW m^{-2})	TTI (s)	t_{PHRR} (s)	THR (MJ/m^{-2})	FGI (kW m^{-2} s^{-1})	COP (g s^{-1})	CO_2P (g s^{-1})
PA6	514.3	91.6	210	126.8	2.44	0.0057	0.501
PA6/ITS-GO-10%	477.6	87.2	171	113.9	2.71	0.0050	0.425
PA6/m-PZS-10%	438.3	86.5	214	117.1	2.04	0.0048	0.454
PA6/PSGO-3%	355.4	79.8	200	102.7	1.77	0.0054	0.326
PA6/PSGO-5%	337.5	72.3	240	94.60	1.40	0.0048	0.292
PA6/PSGO-10%	279.2	63.1	205	86.25	1.36	0.0037	0.243

Abbreviations: CO_2P, CO_2 production; COP, CO production; FGI, fire growth index (FGI = pHRR/tPHRR); pHRR, peak heat release rate; THR, total heat release; TTI, time to ignition.

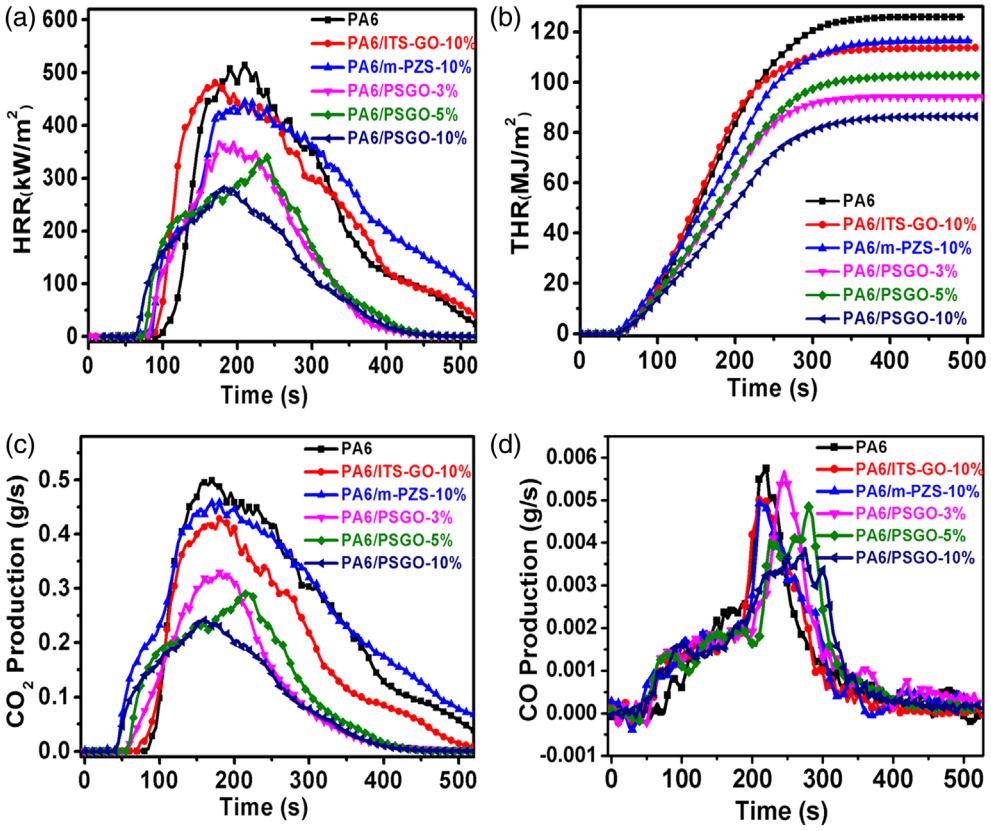

FIGURE 8 Cone calorimetry plots of pristine PA6 and its composites; (a) HRR, (b) THR, (c) CO_2P and (d) COP versus burning time [Color figure can be viewed at wileyonlinelibrary.com]

PA6 composite with 10 wt% PSGO was 279.2 kW m^{-2}, which was significantly (45.7%) lower than that of pristine PA6. Similarly, the PA6/PSGO composites exhibited a noticeable reduction in the THR values with an increase in the PSGO content, as shown in Figure 8b. The THR value for PA6/PSGO-10% composite was 86.25 MJ/m^{-2}, which corresponds to a 36.9% reduction from the 126.8 MJ m^{-2} for pristine PA6. This is mainly attributed to the synergistic effect of m-PZS and ITS-GO, which is involved in the formation of P, N, and Si-containing strong cross-linked char, that contributes to the physical barrier, inhibiting heat evolution during combustion. Moreover, previous studies have confirmed that the gradients of heat release curves are related to the flame spread rate.[45]

Therefore, with decreased $_{p}$HRR and THR values during combustion, the PA6/PSGO-10% composite exhibited excellent FR activity.

The toxic gases released during combustion pose health and safety hazards and are therefore important factors in evaluating the performance of FR materials. The CO is a known toxic gas, and when combined with other gases such as HCN, it becomes more toxic. Hence, the analysis of CO production is important for evaluating

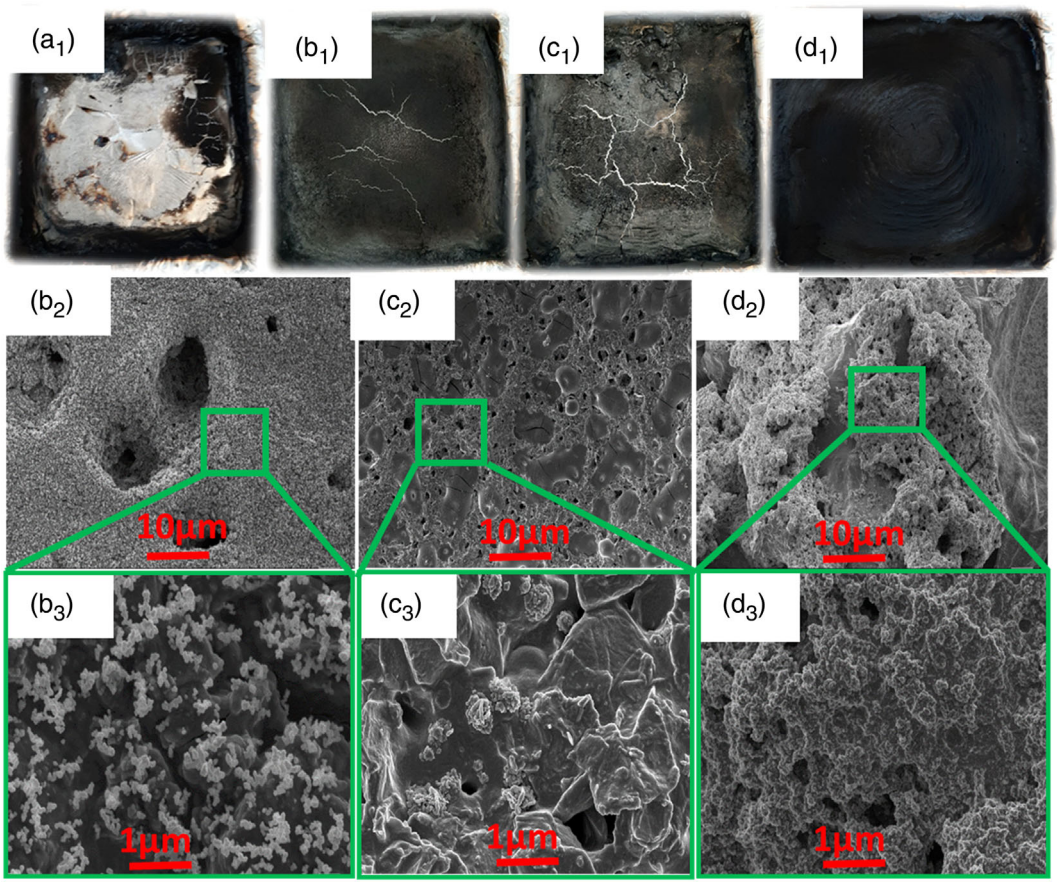

FIGURE 9 The digital photographs and corresponding FESEM images of char residues obtained from cone calorimetry test (a_1) PA6; (b_1, b_2, b_3) PA6/ITS-GO-10%; (c_1, c_2, c_3) PA6/m-PZS-10%; and (d_1, d_2, d_3) PA6/PSGO-10% composites. Digital images credit: Kuruma Malkappa (first author) [Color figure can be viewed at wileyonlinelibrary.com]

the fire safety of polymers. Figure 8c,d show the CO_2 production (CO_2P) and CO production (COP) plots of pristine PA6 and its FR-containing composites. As predicted, Figure 8c,d show that the CO_2P and COP of the PA6 composites are apparently more inhibited by the introduction of various FR compounds compared to those of pristine PA6; the inhibition was more significant in the case of the PSGO composites. The CO_2P and COP of the PA6 composite with 10 wt% PSGO decreased by 43.75% and 60.67%, respectively, when compared with those of pristine PA6. The fire growth index (FGI) is also an important parameter for estimating the flame spread rate in the analysis of polymer fire safety. The FGI values obtained from the cone calorimetry test are included in Table 3; the FGI values are significantly decreased from 2.44 kW m^{-2} s^{-1} for pristine PA6 to 1.36 kW m^{-2} s^{-1} for PA6/PSGO-10% composite. However, in the case of the PA6/ITS-GO composite, the FGI value increased slightly to 2.71 kW m^{-2} s^{-1} owing to the formation of inferior quality char during combustion. Overall, the result indicates that the fire safety of PA6 was considerably improved in the presence of the hybrid FR PSGO.

Characterization of the morphology and chemical composition of the char residues is important because it provides insight into the efficacy of the FRs and helps elucidate the flame retardancy mechanism. Digital photographs of the char residues obtained from cone calorimetry and SEM micrographs of the exterior char residues are presented in Figure 9. First, the digital photograph of the pristine PA6 char residue shown in Figure 9a_1 shows a fragile fluffy thin char layer. In contrast, the amount of char residues obtained from the PA6 composites with ITS-GO and m-PZS increased, but were loose and porous, as shown in Figure 9b_1,c_1. With the addition of PSGO to PA6, a significant increase in the amount of char residues was observed, which appeared thicker and more compact, as shown in Figure 9d_1. The thicker char residues in the PSGO-containing composites suggest that during combustion, improved char formation results in an improved barrier to oxygen ingress to the underlying PA6 matrix, thereby slowing the rate of combustion. The char morphology in Figure 9b_2, b_3 clearly shows that the char formed in the presence of m-PZS contains SiO_2 nanoparticles, which act as thermal insulators in the char layer.

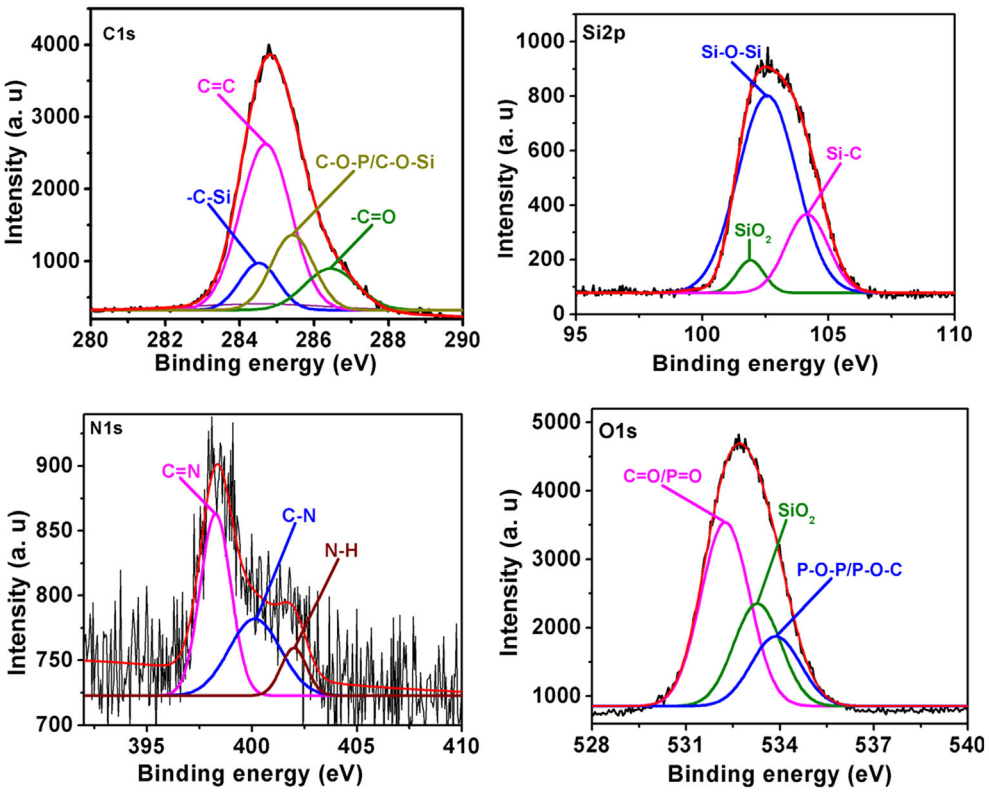

FIGURE 10 The PA6/PSGO-10% composite char residue high-resolution XPS spectra of C 1s, O 1s, Si 2p, and N 1s. [Color figure can be viewed at wileyonlinelibrary.com]

Thus, the composite material is protected from further combustion. The char morphologies of PA6/ITS-GO-10% are shown in Figure 9c$_1$,c$_2$. The presence of some cracks and voids indicates that the char is not strong enough to effectively retard the emission of volatiles from the PA6 matrix and the transmission of heat and oxygen into the matrix. However, the morphology of the PA6/PSGO-10% composite, shown in Figure 9d$_2$,d$_3$, indicates the formation of a more compact and dense char layer with no visible cracks. The strong char formation can be attributed to the wrinkled graphene sheets with cross-linked urethane-siloxane PZS joining each other to form a dense and strengthened char layer, which act as a strong barrier and contribute to the excellent FR activity.

The XPS spectral analysis of the char residue for the PA6/PSGO-10% composite and the decoupled high-resolution spectra of C 1s, Si 2p, O 1s, and N 1s are presented in Figure 10. The peaks in the C 1s spectrum were observed at 284.2, 284.8, 285.3, and 286.7 eV, corresponding to C═C, C—O—P/C—O–Si, —C═O, and C–Si bonds, respectively. The Si 2p spectrum shows peaks at 101.6, 102.2, and 103.8 eV corresponding to Si—O—Si, SiO_2, and Si—C, respectively, indicating the formation of silica-containing cross-linked char. The O 1s spectrum is divided into three clear peaks at 531.8, 532.6, and 533.9 eV, corresponding to P═O/C═O, SiO_2, and P—O—P/P—O—C, respectively, implying the formation of P- and Si-containing cross-linked char. Similarly, the N 1s spectrum is also divided into three peaks at 398.5, 400.9, and 401.9 eV for —C═N, C—N, and N—H, respectively. This can be attributed to the formation of cross-linked char with PZS and PA6 in the composite during combustion. These results clearly indicate that the PSGO hybrid FR containing the PA6 composite can form a highly graphitized cross-linked char during combustion with a combination of multiple elements, such as P, N, O, S, and Si to yield a strong FR activity.

Raman spectroscopy was carried out to investigate the degree of graphitization of the char residues obtained from cone calorimetry analysis. Figure 11a–c show the obtained Raman spectra of the char residues for the PA6 composites with different FR contents. The degree of graphitization of all the char residues was investigated using the integral peak area ratios of the D and G absorption peaks, which appeared at approximately 1365 and 1595 cm^{-1}, respectively, for all the PA6 composite samples. The degree of graphitization of char residues can be analyzed based on the I_D/I_G values, where a lower value represents a higher degree of graphitization of the char residues, which can provide higher thermal stability. For the PA6/ITS-GO-10%, PA6/m-PZS-10%, and PA6/PSGO-10% composite char residues, the I_D/I_G values were 1.25, 1.14, and 0.96, respectively. This indicates that in the presence of the hybrid FR PSGO, the I_D/I_G value for PA6 composite decreased. This is because the combination of m-PZS and ITS-GO with siloxane functionalities helps to

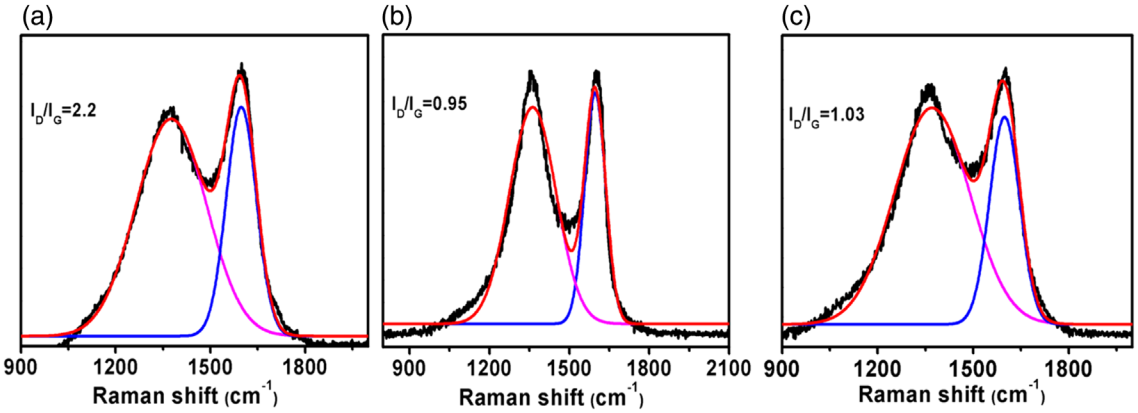

FIGURE 11 Raman spectra of the char residues of PA6 flame retardant composites (a) PA6/ITS-GO-10% (a), PA6/m-PZS-10% (b), and PA6/PSGO-10% (c). [Color figure can be viewed at wileyonlinelibrary.com]

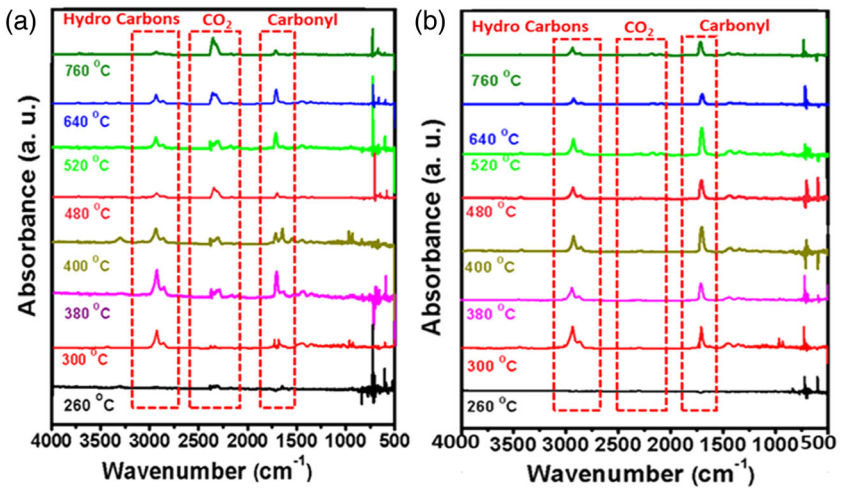

FIGURE 12 The FTIR spectra of released pyrolysis components during thermal degradation of (a) PA6 and (b) PA6/PSGO-10% composite at various temperatures. [Color figure can be viewed at wileyonlinelibrary.com]

form more graphitic char residue, which contributes to the superior flame-retardant activity.

3.5 | Analysis of released pyrolysis products from the PA6 composites

To further evaluate the thermal degradation mechanism and pyrolysis behavior of PA6 and its composites in the presence of various FRs, the released pyrolysis volatile components and toxic gases were analyzed using the TG-FTIR technique. Figure 12a,b show the FTIR spectra of the released pyrolysis components of the PA6 and PA6/PSGO-10% composites at various temperatures. It is clearly seen that the FTIR spectra of PA6/PSGO-10% composite are similar to that of pristine PA6, except for small differences that are observed in the degradation path and peak intensities. The main characteristic released pyrolysis compounds of PA6 and PA6/PSGO-10% FR composites were identified based on the absorption peaks at 1540 cm^{-1} (aromatic compounds), 1746 cm^{-1} (carbonyl compounds), 2800–2900 cm^{-1} (hydrocarbons), and 958 cm^{-1} (ammonia). To compare the changes in the release volume of all pyrolytic gas components, the Gram–Schmidt plots of PA6 and its composites with different FRs are shown in Figure 13a. The absorbance intensity of the PA6/PSGO-10% composite was much lower than that of pristine PA6 and its composites with ITS-GO and m-PZS. This is mainly attributed to the formation of highly cross-linked char with combinations of P, N, S, and Si, which are strong and capable of providing good barrier properties. This prevents the release of unstable volatile organic compounds and toxic gases. Moreover, in the PA6/PSGO-10% composite, the decrease in the release of pyrolysis components was observed comparatively earlier than that for pristine PA6, indicating the catalysis of the PA6 thermal degradation process in the presence of hybrid FR PSGO. Similarly, all other individual absorbance plots of the released pyrolytic components versus time are presented in Figure 13 (b, hydrocarbons; c, CO; and d, CO_2). The absorbance intensities of the released pyrolytic

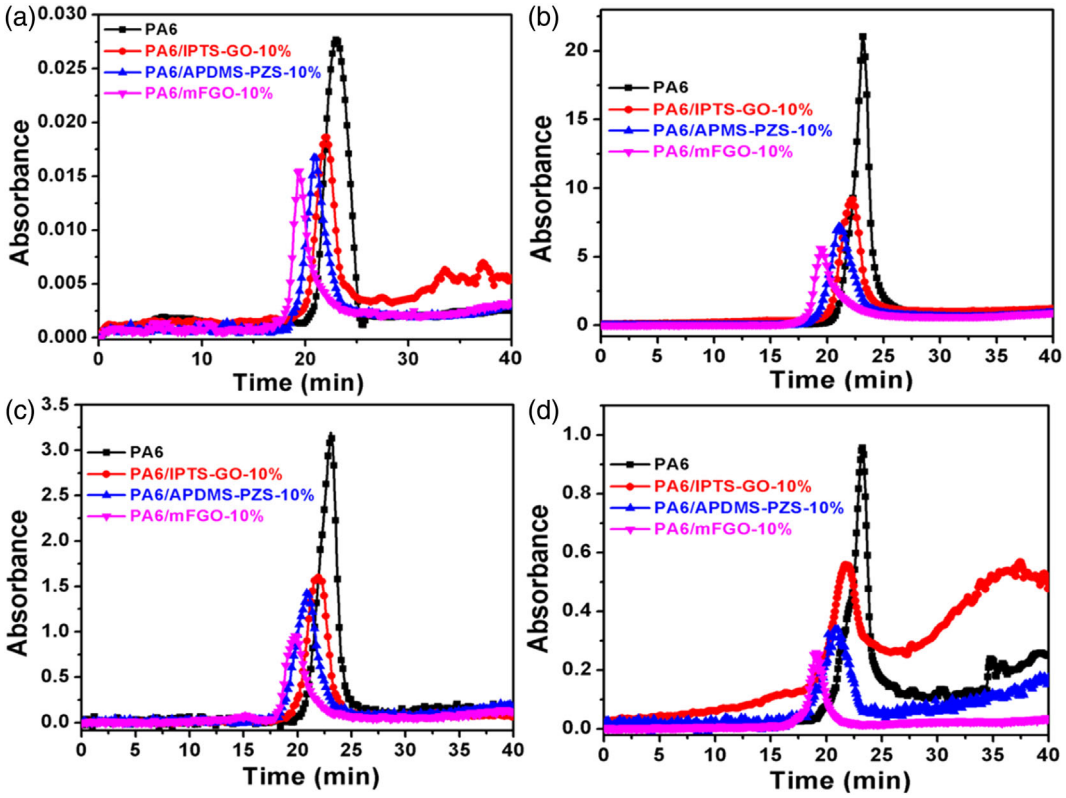

FIGURE 13 Absorbance plots of released pyrolysis components versus time for PA6 and its composites with different FRs; (a) gram–Schmidt plots, (b) hydrocarbons, (c) CO, and (d) CO_2 [Color figure can be viewed at wileyonlinelibrary.com]

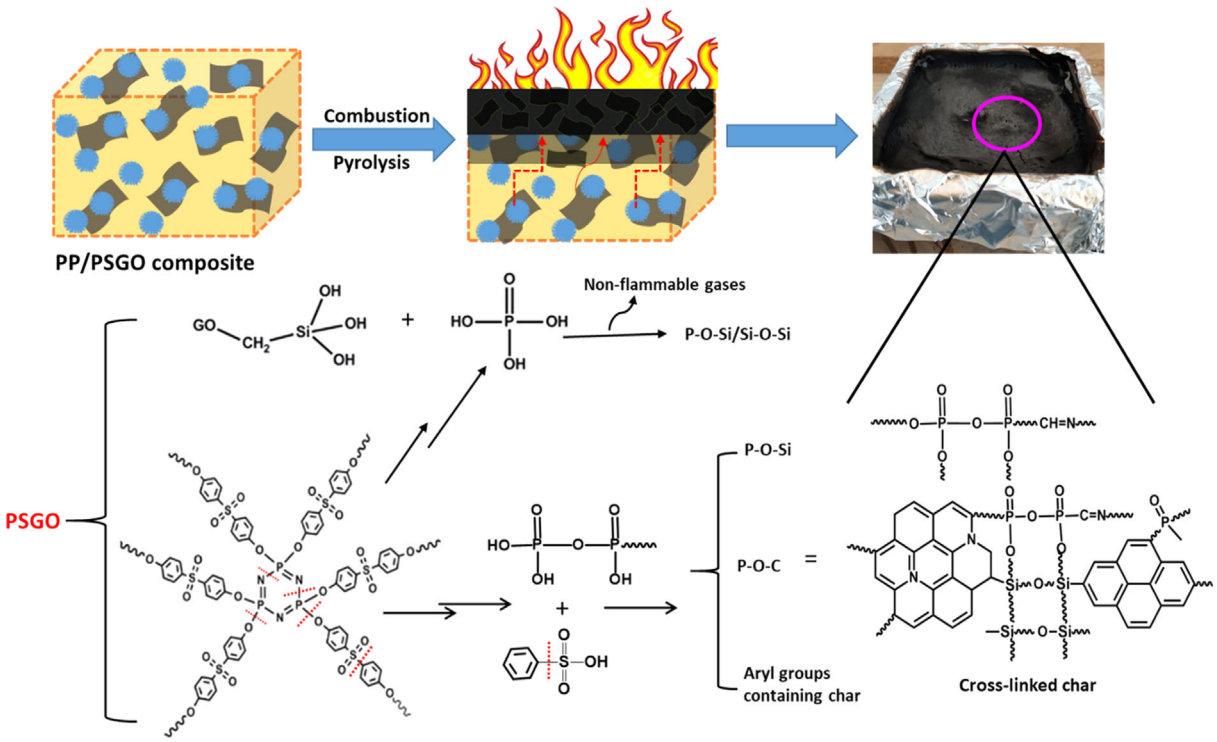

FIGURE 14 Illustration of FR mechanism and cross-linked char formation during combustion. [Color figure can be viewed at wileyonlinelibrary.com]

components for the PA6/PSGO-10% composite were lower than those of the pristine PA6, PA6/ITS-GO, and PA6/m-PZS composites. The decrease in the evolution of volatile organic compounds indicates a good FR performance of the PSGO-containing PA6 composite. During fire, the evolution of all these volatile organic compounds not only promote combustion but are also responsible for the formation of smoke particles upon cooling, which increases the fire risk. Therefore, the reduced fire hazards of PSGO-containing PA6 composite can be attributed to the possible synergistic effect of the ITS-GO nanosheets and m-PZS, which promotes the formation of highly cross-linked char by further decreasing the thermal decomposition and gas diffusion rate.

Based on the aforementioned analysis, a possible FR mechanism of PSGO in the PA6 composite is proposed in Figure 14. The main reason for the enhancement of the FR activity along with the release of smoke and organic volatiles in the PA6/PSGO composite is the synergetic charring effect between m-PZS and ITS-GO, and the physical barrier effect of graphene nanosheets. Moreover, the hybrid FR PSGO nanosheets were well-distributed in the PA6 matrix through strong interfacial interactions between the amide groups of PA6 and the PSGO hybrid. Hence, the PSGO graphene sheets play a strategic role in barrier properties, not only preventing oxygen infiltration, but also preventing the diffusion of heat and mass and the release of small organic volatile components from the underlying polymer material. Contrastingly, during the combustion of the PA6/PSGO composite, the grafted branched APTES/PDMS siloxane units of m-PZS on graphene sheets, which were formed due to thermal oxidative degradation, were gradually converted into Si–O–Si units containing a network, and then rapidly transformed into SiO_2 particles, as shown in Figure 9b_2, b_3. Additionally, the PZS units also decomposed into the P–N–S containing a strong barrier layer on the surface of the graphene sheets. These two factors are more important for increasing the insulating nature of char and compactness of graphene nanosheets during combustion, thereby providing strong barrier properties to inhibit the evolution of volatile organic components even at higher temperatures. Moreover, owing to the presence of more phenyl groups along with graphene sheets that rapidly transformed into char residues (Figure 14), the resulting rigid char played a vital role in enhancing the flame retardancy of PA6 in the condensed phase.

4 | CONCLUSION

In summary, a novel graphene-based organic/inorganic hybrid FR (PSGO) material integrating P, N, S, and Si was successfully synthesized via a sol–gel surface modification method. The structure of the PSGO FR was confirmed by FTIR, XRD, SEM, and TEM. A series of PA6 composites based on m-PZS, ITS-GO, and varying percentages of hybrid PSGO FRs were prepared using the melt-processing method. The flame retardancy and thermomechanical properties of the composites were compared. Specifically, the PA6/PSGO composites exhibited excellent flame retardancy and mechanical properties compared to those of the individual ITS-GO and m-PZS containing PA6 composites. In addition, it was observed that with an increase in the PSGO content in the polymer matrix, both the FR property and the elastic modulus (E′) increased. The PA6 composite with 10 wt% of PSGO content showed significantly decreased $_{p}$HRR and THR values of 279.2 kW m^{-2} and 86.25 MJ m^{-2}, respectively, compared to those for pristine PA6 (514.3 kW m^{-2} and 126.8 MJ/m^{-2}, respectively). This corresponds to a decrease of 45.7% and 36.9% in the pHHR and THR values, respectively. These attractive properties are attributed to the resistance to the thermal-oxidative degradation of PSGO and improved interfacial interactions with the polymer matrix. Interestingly, PSGO can be used as a multifunctional modifier to improve the thermal, mechanical, and FR properties. Moreover, it was confirmed that 10 wt% of PSGO in the PA6 composite is sufficient to yield excellent water resistance and superior flame retardancy of the composite, resulting in a V–0 rating for the UL-94 test even after the water immersion test. From TG-FTIR/GC–MS, it was confirmed that 10% PSGO in PA6 significantly inhibited the release of small organic volatiles and toxic gases during combustion. This is attributed to the formation of P–N–Si-containing cross-linked compounds with graphene, which provide strong barrier properties. In conclusion, the multifunctional, novel PSGO hybrid FR is suitable for flame retardancy in the PA6 matrix and can synergistically enhance the mechanical properties and hydrophobicity of the composite.

AUTHOR CONTRIBUTIONS

Kuruma Malkappa: Conceptualization (lead); formal analysis (lead); writing – original draft (lead). **Jayita Bandyopadhyay:** Conceptualization (equal); project administration (equal); supervision (equal); writing – review and editing (equal). **Vincent Ojijo:** Project administration (supporting); supervision (supporting); writing – review and editing (supporting).

ACKNOWLEDGMENTS

The authors would like to acknowledge the financial support from the Department of Science and Innovation (C6ACH35), Council for Scientific and Industrial

Research, Pretoria (086ADMIN), and the University of Johannesburg, South Africa (086310).

CONFLICT OF INTEREST

The authors declare no conflicts of interest.

DATA AVAILABILITY STATEMENT

Research data are not shared.

ORCID

Jayita Bandyopadhyay https://orcid.org/0000-0002-6330-113X
Suprakas Sinha Ray https://orcid.org/0000-0002-0007-2595

REFERENCES

[1] H. Meng, G. Sui, G. Xie, R. Yang, *Compos. Sci. Technol.* **2009**, *69*, 606.
[2] K. Malkappa, S. S. Ray, *ACS Omega* **2019**, *4*, 9615.
[3] S. V. Levchik, E. D. Weil, *Polym. Inter.* **2000**, *49*, 1033.
[4] X. Hao, G. Gai, J. Liu, Y. Yang, Y. Zhang, C.-W. Nan, *Mater. Chem. Phys.* **2006**, *96*, 34.
[5] L. Song, Y. Hu, Z. Lin, S. Xuan, S. Wang, Z. Chen, W. Fan, *Polym. Degrad. Stab.* **2004**, *86*, 535.
[6] W. Du, Y. Jin, S. Lai, L. Shi, Y. Shen, J. Pan, *Appl. Surf. Sci.* **2019**, *492*, 298.
[7] Y. Zhang, B. Wang, B. Yuan, Y. Yuan, K. M. Liew, L. Song, Y. Hu, *Ind. Eng. Chem. Res.* **2017**, *56*, 7468.
[8] S. Khanal, Y. Lu, D. Jin, S. Xu, *Fire Mater.* **2022**, *46*, 107.
[9] X. Feng, X. Wang, W. Cai, N. Hong, Y. Hu, K. M. Liew, *J. Hazard. Mater.* **2016**, *320*, 252.
[10] K. Malkappa, R. Salehiyan, S. S. Ray, *Macromol. Mater. Eng.* **2020**, *305*, 2000207.
[11] Y. Feng, C. He, Y. Wen, Y. Ye, X. Zhou, X. Xie, Y.-W. Mai, *Compos. Part A: Appl. Sci. Manuf.* **2017**, *103*, 74.
[12] Y. Sui, L. Qu, P. Li, X. Dai, Q. Fang, C. Zhang, Y. Wang, *RSC Adv.* **2020**, *10*, 13949.
[13] G.-R. Xu, M.-J. Xu, B. Li, *Polym. Degrad. Stab.* **2014**, *109*, 240.
[14] H. Liu, X. Wang, D. Wu, *Polym. Degrad. Stab.* **2014**, *103*, 96.
[15] L. Qu, Y. Sui, C. Zhang, P. Li, X. Dai, B. Xu, *React. Funct. Polym.* **2020**, *155*, 104697.
[16] F. Feng, C. He, Y. Wen, Y. Ye, X. Zhou, X. Xie, Y.-W. Mai, *J. Hazard. Mater.* **2018**, *346*, 140.
[17] W. Cai, J. Wang, Y. Pan, W. Guo, X. Mu, X. Feng, B. Yuan, X. Wang, Y. Hu, *J. Hazard. Mater.* **2018**, *352*, 57.
[18] W. Hu, B. Yu, S.-D. Jiang, L. Song, Y. Hu, B. Wang, *J. Hazard. Mater.* **2015**, *300*, 58.
[19] W. Zhou, H. Yang, *Thermochim. Acta* **2007**, *452*, 43.
[20] X. Qian, B. Yu, C. Bao, L. Song, B. Wang, W. Xing, Y. Hu, R. K. Yuen, *J. Mater. Chem. Part A* **2013**, *1*, 9827.
[21] Z. Wang, P. Wei, Y. Qian, J. Liu, *Compos. Part B Eng.* **2014**, *60*, 341.
[22] R. Wang, D. Zhuo, Z. Weng, L. Wu, X. Cheng, Y. Zhou, J. Wang, B. Xuan, *J. Mater. Chem. Part A* **2015**, *3*, 9826.
[23] C. Tang, H. Yan, S. Li, M. Li, Z. Chen, *J. Polym. Res.* **2017**, *24*, 1.
[24] S. Fan, B. Peng, R. Yuan, D. Wu, X. Wang, J. Yu, F. Li, *Compos. Part B Eng.* **2020**, *183*, 107684.
[25] D. Lin, X. Zeng, H. Li, X. Lai, *Cellul.* **2018**, *25*, 3135.
[26] W. Guo, X. Wang, J. Huang, Y. Zhou, W. Cai, J. Wang, L. Song, Y. Hu, *Chem. Eng. J.* **2020**, *398*, 125661.
[27] Y. Pan, L. Song, W. Wang, H. Zhao, *J. Appl. Polym. Sci.* **2020**, *137*, 49027.
[28] M. J. Xu, C. Liu, K. Ma, Y. Leng, B. Li, *Polym. Adv. Technol.* **2017**, *28*, 1382.
[29] M. Mao, H. Xu, K.-Y. Guo, J.-W. Zhang, Q.-Q. Xia, G.-D. Zhang, L. Zhao, J.-F. Gao, L.-C. Tang, *Compos. Part A: Appl. Sci. Manuf.* **2021**, *140*, 106191.
[30] K.-Y. Guo, Q. Wu, M. Mao, H. Chen, G.-D. Zhang, L. Zhao, J.-F. Gao, P. Song, L.-C. Tang, *Compos. Part B Eng.* **2020**, *193*, 108017.
[31] H. Fang, Y. Zhao, Y. Zhang, Y. Ren, S.-L. Bai, A. C. S. Appl, *Mater. Interfaces* **2017**, *9*, 26447.
[32] M. Yu, F. Liu, F. Du, *Prog. Org. Coat.* **2016**, *94*, 34.
[33] D. C. Marcano, D. V. Kosynkin, J. M. Berlin, A. Sinitskii, Z. Sun, A. Slesarev, L. B. Alemany, W. Lu, J. M. Tour, *ACS Nano* **2010**, *4*, 4806.
[34] S. Qiu, C. Ma, X. Wang, X. Zhou, X. Feng, R. K. Yuen, Y. Hu, *J. Hazard. Mater.* **2018**, *344*, 839.
[35] X. Zhou, S. Qiu, W. Xing, C. S. R. Gangireddy, Z. Gui, Y. Hu, A. C. S. Appl, *Mater. Interfaces* **2017**, *9*, 29147.
[36] C. L. Chiang, S. W. Hsu, *Polym. Inter.* **2010**, *59*, 119.
[37] M. Yoonessi, J. R. Gaier, *ACS Nano* **2010**, *4*, 7211.
[38] S. Roy, X. Tang, T. Das, L. Zhang, Y. Li, S. Ting, X. Hu, C. Yue, A. C. S. Appl, *Mater. Interfaces* **2015**, *7*, 3142.
[39] V. H. Pham, T. V. Cuong, T. T. Dang, S. H. Hur, B.-S. Kong, E. J. Kim, E. W. Shin, J. S. Chung, *J. Mater. Chem.* **2011**, *21*, 11312.
[40] W. Du, Y. Jin, S. Lai, L. Shi, Y. Shen, H. Yang, *Compos. Part A: Appl. Sci. Manuf.* **2020**, *128*, 105686.
[41] Q. Tian, Y. C. Yuan, M. Z. Rong, M. Q. Zhang, *J. Mater. Chem.* **2009**, *19*, 1289.
[42] K. Malkappa, J. Bandyopadhyay, S. S. Ray, *ACS Omega* **2017**, *5*, 13867.
[43] S. Gao, B. Li, P. Bai, S. Zhang, *Polym. Adv. Technol.* **2011**, *22*, 2609.
[44] J. Ni, L. Chen, K. Zhao, Y. Hu, L. Song, *Polym. Adv. Technol.* **2011**, *22*, 1824.
[45] M. Zhang, X. Ding, Y. Zhan, Y. Wang, X. Wang, *J. Hazard. Mater.* **2020**, *384*, 121260.

How to cite this article: K. Malkappa, J. Bandyopadhyay, V. Ojijo, S. S. Ray, *J. Appl. Polym. Sci.* **2022**, *139*(37), e52867. https://doi.org/10.1002/app.52867